Received: 7 December 2024 | Accepted: 16 January 2025

DOI: 10.1097/HC9.0000000000000674

ORIGINAL ARTICLE

OPEN

EBV enhances immunotherapy sensitivity in intrahepatic cholangiocarcinoma through cGAS-STING pathway activation

Lingli Huang[1,2,3,4] | **Qian Zhong**[2,3,4,5] | **Silan Huang**[1,2,3,4] | **Kejia Yang**[1,2,3,4] | **Yuchen Cai**[2,3,4,5] | **Guifang Guo**[1,2,3,4]

[1]VIP Department, Sun Yat-sen University Cancer Center, Guangzhou, P.R. China

[2]State Key Laboratory of Oncology in South China, Sun Yat-sen University Cancer Center, Guangzhou, P.R. China

[3]Collaborative Innovation Center for Cancer Medicine, Sun Yat-sen University Cancer Center, Guangzhou, P.R. China

[4]Guangdong Provincial Clinical Research Center for Cancer, Sun Yat-sen University Cancer Center, Guangzhou, P.R. China

[5]State Key Laboratory of Oncology, Experimental Research Department, Sun Yat-sen University Cancer Center, Guangzhou, P.R. China

Correspondence
Guifang Guo, VIP Department, Sun Yat-sen University Cancer Center, 651 Dongfeng Road East, Guangzhou 510060, P.R. China.
Email: guogf@sysucc.org.cn

Yuchen Cai, State Key Laboratory of Oncology in South China, Experimental Research Department, Sun Yat-sen University Cancer Center, 651 Dongfeng Road East, Guangzhou 510060, P.R. China.
Email: caiych@sysucc.org.cn

Abstract

Background: The absence of representative Epstein-Barr virus–associated intrahepatic cholangiocarcinoma (EBVaICC) cell lines has limited our understanding of the molecular and immunological characteristics of this cancer subtype.

Methods: We reviewed patients with metastatic cholangiocarcinoma at Sun Yat-sen University Cancer Center from January 2015 to August 2023. Among them, 22 patients with EBVaICC and 66 patients with non-EBVaICC who received anti-PD1 treatment were included. Additionally, 2 EBV-positive ICC cell lines, RBE-EBV and HuH28-EBV, were developed through cell-to-cell infection. Stable EBV infection and responsiveness to viral reactivation were confirmed. Transcriptomic and bioinformatics analyses were performed, and in vitro experiments examined the immune effects of EBV-positive ICC. Key immune-related genes and cytokines were validated by reverse transcription quantitative polymerase chain reaction and ELISA in cell lines and patient plasma samples.

Results: In this study, we found that patients with EBVaICC showed enhanced immune responses and improved overall and progression-free survival compared to patients with non-EBVaICC. We first successfully established and validated 2 EBV-positive ICC cell lines (RBE-EBV and HuH28-EBV). These cell lines were confirmed for stable EBV infection and displayed responsiveness to viral reactivation, making them suitable for future studies. Transcriptomic analyses and in vitro studies revealed that EBV activated the cGAS-STING pathway, resulting in MHC-I upregulation and CXCL10 secretion in ICC cells, which collectively enhanced CD8+ T cell chemotaxis and cytotoxicity.

Abbreviations: BTC, biliary tract cancer; cGAMP, 2′3′-cyclic GMP-AMP; cGAS-STING, 2′3′-cyclic GMP-AMP synthase–stimulator of interferon genes; CXCL10, C-X-C motif chemokine ligand 10; DC, dendritic cells; EBVaICC, Epstein-Barr virus–associated intrahepatic cholangiocarcinoma; PBMC, peripheral blood mononuclear cells; PD1, programmed cell death protein 1; TPA, phorbol 12-myristate 13-acetate.

Lingli Huang, Qian Zhong, and Silan Huang contributed equally to this work.

Supplemental Digital Content is available for this article. Direct URL citations are provided in the HTML and PDF versions of this article on the journal's website, www.hepcommjournal.com.

Furthermore, ELISA analysis showed higher plasma levels of CXCL10 and IFN-γ in patients with EBVaICC, suggesting a potential role for EBV in enhancing immunotherapy sensitivity in this subtype.

Conclusions: The established EBV-positive ICC cell lines revealed enhanced immunogenicity driven by cGAS-STING pathway activation, providing valuable models for future research and insights into the mechanisms of improved immunotherapy sensitivity in EBVaICC.

Keywords: cGAS-STING, Epstein-Barr virus, immunotherapy, interferon, intrahepatic cholangiocarcinoma

INTRODUCTION

Biliary tract cancer (BTC) is a group of malignancies with rising incidence and poor prognosis, contributing to high mortality rates.[1] Most BTC cases are diagnosed at an advanced stage, which precludes curative surgery and leaves few treatment options available. Although recent advancements in immunotherapy combined with chemotherapy have offered new hope for patients with advanced BTC, the median overall survival remains limited to 12.8 months.[2,3] The etiology and risk factors associated with BTC are still incompletely understood.[4] BTC encompasses multiple subtypes based on anatomical location, including intrahepatic cholangiocarcinoma (ICC), perihilar cholangiocarcinoma, and distal cholangiocarcinoma, each exhibiting distinct genomic characteristics, molecular alterations, and therapeutic responses.[5,6] However, for patients with BTC without specific biomarkers of immunotherapy, effective therapeutic strategies are urgently needed.

Recent studies have identified a unique subtype of ICC, Epstein-Barr virus–associated intrahepatic cholangiocarcinoma (EBVaICC), which is characterized by a distinct immune microenvironment and significant CD8+ T-cell infiltration.[7] Although the treatment regimen for EBVaICC is consistent with that for ICC, patients with EBVaICC have demonstrated a favorable response to anti-programmed cell death protein 1 (PD1) immunotherapy and exhibit better survival outcomes compared to those with ICC.[8] However, the low prevalence of EBVaICC, along with challenges in model construction, has hampered in vitro studies, resulting in a largely unexplored pathway regarding EBV infection of ICC and its mechanisms for modulating immunotherapy and remodeling the tumor immune microenvironment.

EBV is a common γ-herpesvirus that primarily infects B lymphocytes and epithelial cells. It is associated with the treatment outcomes and prognosis of various malignant tumors.[9,10] In nasopharyngeal carcinoma, EBV promotes the production of IFN-α by plasmacytoid dendritic cells, enhancing natural killer cell cytotoxicity.[11,12] Additionally, EBV dUTPase activates the MyD88-dependent NF-κB pathway in macrophages, leading to the induction of TNF-α, IL-1β, and IL-6 expression.[13,14] EBV-related antigens also act as neoantigens, inducing EBV-specific cytotoxic T lymphocytes, although the specific role of EBV-driven immune responses in nasopharyngeal carcinoma is not fully understood.[15] EBV-associated gastric carcinomas frequently exhibit high PD-L1 expression, accompanied by infiltration of CD8+ cytotoxic T lymphocytes and mature dendritic cells, thereby establishing EBV as a potential biomarker in this context. Similarly, our previous study demonstrated that the expression levels of CD3 and CD8 in the tumor regions of patients with EBVaICC were higher than those in patients with mismatch repair-deficient BTC, with differential protein enrichment primarily related to T-cell activation.[8] Therefore, it is crucial to further investigate the mechanisms underlying the favorable immune response observed in EBVaICC.

Acute activation of the innate immune system establishes the foundation for a more complex adaptive immune response, with the maturation and migration of dendritic cells (DCs) presenting antigens to activate T cells.[15] As an important second messenger, 2′3′-cyclic GMP-AMPs (cGAMP) serves as a key sensing mechanism for intracellular DNA, activating the 2′3′-cyclic GMP-AMP synthase–stimulator of interferon gene (cGAS-STING) pathway to induce type I interferon and proinflammatory cytokine expression, thereby triggering immune defense mechanisms.[16,17] In contrast, previous studies have shown that EBV can activate CD47 expression via the cGAS-STING pathway, inhibiting macrophage phagocytosis.[18] Furthermore, EBV deubiquitinase BPLF1 reduces type I interferon production through the cGAS-STING and RIG-I-MAVS pathways.[19] These findings suggest that the cGAS-STING pathway may play a crucial role in EBV-associated cancer and warrants further investigation.

Based on this, the present study aims to establish and validate an EBV-positive ICC cell line model to

investigate the molecular and immunological features of this tumor subtype. We specifically focus on elucidating the mechanisms underlying the sensitivity of EBV-positive ICC to immunotherapy. Through this study, we hope to reveal key immunobiological characteristics of EBV-positive ICC, providing insights for future personalized treatment approaches.

METHODS

Patients and samples

Tissues and plasma from patients with advanced ICC were obtained from the Specimen Resource Library at Sun Yat-sen University Cancer Center (Guangzhou, China). Patients without necessary clinical records or available pathological tumor tissues were excluded. Samples were collected after obtaining written informed consent from the patients, and all related procedures were approved by the Institutional Review Board and Ethics Committee of Sun Yat-sen University Cancer Center, according to the Declaration of Helsinki (Approval No: B2023-231). All tissues from patients with EBVaICC were EBER positive.

Cell lines

The human ICC cell lines (RBE and HuH28) were generously provided by Professor Shengping Li from the Sun Yat-sen University Cancer Center. These cell lines were cultured in RPMI-1640 medium (Gibco) supplemented with 10% fetal bovine serum (Gibco, South America) and 1% antibiotics (penicillin and streptomycin, Gibco). Raji cells and Akata cells infected with recombinant EBV were a kind gift from Professor Musheng Zeng (Sun Yat-sen University Cancer Center). These were cultured in RPMI-1640 containing 700 μg/mL G418 (MP, USA). The EBV-infected ICC cell lines, RBE-EBV and HuH28-EBV, were cultured in a selective medium containing 500 μg/mL G418. All cells were maintained in a 37 °C, 5% CO_2 environment. All cells were maintained within 10 passages, and EBV-infected cells were routinely assessed using EBER in situ hybridization (EBER-ISH).

Establishment of EBV-infected ICC cell lines

This study used a cell-to-cell method for the in vitro EBV infection of ICC cell lines.[20] Briefly, EGFP-neo EBV-infected Akata cells were used to produce recombinant EBV. Initially, the Akata cell suspension was incubated in a serum-free medium and stimulated with 0.8% (v/v) goat anti-human serum IgG cross-linking to shift the EBV from latency to lytic phase. Next, the cells were washed with PBS to remove serum IgG and co-cultured with ICC cells (RBE and HuH28) for 6 days at a ratio of Akata to ICC cells of 1:5, with media replacement every 2 days. After washing the ICC cells with PBS, they were selected in a medium containing 500 μg/mL G418 for 3 weeks.

EBV lytic induction

For EBV lytic induction, 2×10^5 logarithmic growth phase RBE-EBV and HuH28-EBV cells were seeded in 6-well plates. After 24 hours, cells were treated with phorbol 12-myristate 13-acetate (TPA, 20 ng/mL) and Sodium butyrate (NaB, 3 mM) incubated for 0, 12, 24, and 48 hours, respectively. Following the EBV lytic cycle induction, cells were collected for the next experiment.

EBER in situ hybridization

The detection of EBERs was performed using an EBER in situ hybridization kit according to the manufacturer's instructions (ZSGB-BIO). In brief, paraffin sections were deparaffinized, and adherent cells were digested and evenly spread onto glass slides, followed by fixation with 4% paraformaldehyde. Subsequently, sections were treated with proteinase K, hybridized with digoxigenin-labeled EBER probes, and incubated with anti-digoxigenin IgG/HRP antibodies at 37 °C for 30 minutes. Then, the slides were incubated with DAB solution for color development, and the staining was observed under a microscope, with the reaction halted promptly.

EBV copy number

Supernatants from cells cultured for 48 hours were collected, and DNase I (Thermo Scientific) was used to eliminate free EBV DNA from the culture medium. Subsequently, 0.1 mg/mL proteinase K (20 mg/mL, Cat#RT403-01, TIANGEN) was added at a 1:1 volume ratio to digest the viral capsid, releasing EBV DNA from the nucleocapsid into the supernatant. According to the manufacturer's protocol, genomic DNA was extracted from cell lines using a DNA extraction kit (TIANGEN, cat#DP304-02). Real-time fluorescence quantitative PCR was performed using BamH I-W and β-globin primers, along with SuperReal PreMix (Probe) (TIANGEN; cat# FP206). The sequences of the primers and probes are as follows: BamHI-W: W-44F: CCCAACACTCCACCACACC; W-119R: TCTTAGGAGCTGTCCGAGGG; Taqman-W-67T: (FAM) CACACACTACACACACCACCAGTCTC (TAMRA); β-globin: β-globin-354F: GTGCATCTGACTCC TGAGGAGA; β-globin-455R: CCTTGATACCAACCTGCC CAG; Taqman-β-globin-402T (FAM) AAGGTGAACGTGG

ATGAAGTTGGTGG (TAMRA). PCR was conducted using DNA from Raji cells to establish a tenfold standard curve. The copy number calculation formula is $C = QBw / [(Q\beta\text{-globin}/2) \times 6.6\times10^{-6}]$, where BW is the EBV DNA copy number determined from the standard curve. qPCR and data analysis were performed using a Bio-Rad CFX96 machine.

Reverse Transcription Quantitative Polymerase Chain Reaction

Total RNA was extracted from cells and tissues using TRIzol (Invitrogen). Complementary DNA was synthesized using a Complementary DNA synthesis kit (Vazyse, Cat# R333-01) following the manufacturer's protocols. qPCR was conducted using SYBR Color qPCR Master Mix (Vazyse, Cat# Q331-02). Reactions were performed in triplicate for 3 independent experiments. Primers for qPCR analysis are shown in Supplemental Table S1, http://links.lww.com/HC9/B936.

Western blot

Total protein was extracted using RIPA buffer (CWBIO, China) supplemented with phosphatase inhibitors. Protein concentrations were measured and adjusted using a BCA Protein Assay Kit (ThermoFisher). Proteins were then separated by SDS-PAGE and transferred to Polyvinylidene Fluoride membranes. Membranes were blocked with 5% non-fat milk at room temperature for 1 hour and incubated overnight at 4 °C with primary antibodies, including against ZEBRA (Zta) (Santa Cruz, cat#sc-53904) or EA-D (Millipore, cat#-MAB8186), GAPDH (Proteintech; cat #10494-1-AP), gp350 (Sino Biological, cat#40373-T62), EBNA1(Santa Cruz, cat#sc-81581), LMP1 (Abcam, cat#ab78113), Phospho-STING (CST, cat#50907), Phospho-TBK1 (CST, cat#5483), Major Histocompatibility Complex Class I (MHC-I) (abcam, cat#ab70328). The secondary antibody was incubated for 1 hour at room temperature, and the bands were visualized using FDbio-Dura ECL reagent (FDbio, Cat# FD8020, China).

Flow cytometry

To detect the expression of gp350 in reactivated RBE-EBV and HuH28-EBV cells, cells were seeded in 6-well plates and allowed to culture for 24 hours. EBV was then reactivated with TPA and NaB for 48 hours. Cells were stained with an anti-gp350 monoclonal antibody, followed by staining with an AlexaFluor594-conjugated secondary antibody. Flow cytometry analysis was performed using a Beckman Coulter FC500.

Immunofluorescence

In total, 5×10^4 cells were seeded in 12-well plates containing cell culture slides. After adherence, 3 mM NaB and 20 ng/mL TPA were added for treatment over 48 hours. The cells were fixed with 4% paraformaldehyde for 30 minutes and then permeabilized with 0.2% Triton-X100 for 10 minutes. Blocking was performed using 5% BSA for 30 minutes. Primary antibodies were incubated at 37 °C for 30–60 minutes, followed by 3 washes with 0.5% BSA. Secondary antibodies were incubated in the dark at room temperature for 30 minutes and stained with 1 μg/mL DAPI for 1 minute, washed 3 times with PBS, each time for 2–3 minutes. After mounting to prevent fluorescence quenching, the samples were observed under a fluorescence microscope. Images were obtained using a confocal microscope (LSM880; Zeiss).

Immunohistochemistry

Cells were evenly spread on slides and fixed, followed by permeabilization and blocking for 1 hour. Primary antibodies were incubated for 1 hour, and secondary antibodies were incubated at 37 °C for 30 minutes. After DAB labeling of antibody binding sites, cell nuclei were stained with hematoxylin. The following primary antibody was used: CK7 (ZSGB-BIO, cat# ZM-0071).

Transcriptome sequencing and analysis

Total RNA was extracted from EBV-negative and EBV-positive cells and tissues using TRIzol reagent according to the manufacturer's protocol. The purity and concentration of total RNA were determined using spectrophotometry. RNA integrity was confirmed through agarose gel electrophoresis. Transcriptome analysis was performed by Nuobiotech (Guangzhou, China). Briefly, mRNA was isolated from total RNA and fragmented. The mRNA fragments were then reverse-transcribed into Complementary DNA to construct the library, followed by paired-end sequencing. Raw data were filtered to obtain more accurate results. Functional enrichment analysis was conducted using the Gene Ontology database, and pathway enrichment analysis was performed using the Kyoto Encyclopedia of Genes and Genomes database.

Peripheral blood mononuclear cells isolation and magnetic bead sorting

Peripheral blood mononuclear cells (PBMCs) were isolated using Ficoll (Cytiva, cat#17544602) density gradient centrifugation. Briefly, anticoagulated peripheral blood from healthy donors was diluted 3-fold with PBS after plasma removal and then added to Ficoll-

filled centrifuge tubes and centrifuged in a density gradient at 800*g* for 25 minutes. The intermediate layer containing PBMCs was collected. Specific immune cell populations were isolated from PBMCs using Miltenyi magnetic cell sorting. PBMCs were resuspended at a concentration of 1×10^7 cells in 80 μL of automatic Miltenyi magnetic cell sorting running buffer. Subsequently, 20 μL of magnetic beads were added and incubated in the dark at 4 °C for 15 minutes. Cells were diluted with Miltenyi magnetic cell sorting buffer and added to a separation column placed in a strong magnetic field. The labeled cells were retained in the column, and after removing the strong magnetic field, the unbound cells were washed away, yielding a specific immune cell population with over 90% purity. CD8 magnetic beads (Miltenyi, cat#130-045-201) were used to sort $CD8^+$ T cells, which were then cultured in an X-vivo medium (LONZA) supplemented with 200 IU/mL IL-2.

T cell cytotoxicity

PBMCs were suspended in serum-free DMEM and seeded at a density of 5×10^6 cells/mL into 6-well plates, adding 2 mL of culture medium per well, and incubated at 37 °C for 30 minutes. The cells were then washed twice with PBS, collected, and cultured in a DC differentiation medium containing 20 ng/mL IL-4 and 50 ng/mL GM-CSF for 7 days, replacing half the medium every 2 days. $CD8^+$ T cells were activated using CD3/CD28, and tumor cells were co-cultured with DCs to promote DC maturation. After maturation, the DCs were co-cultured with $CD8^+$ T cells for 5 days for antigen presentation. Tumor cells were stained with Carboxyfluorescein Diacetate Succinimidyl Ester and co-cultured with activated CD8+T cells for 24 hours. Subsequently, cells were incubated with 5 μL of Annexin V-647 in the dark for 10 minutes, followed by the addition of 5 μL of Propidium Iodide for 5 minutes, and finally analyzed for tumor cell apoptosis using flow cytometry within 30 minutes.

T-cell chemotaxis assay

We used 3 μm Transwell chambers (Corning, Cat#353096) to assess the migratory capacity of $CD8^+$ T cells. Tumor supernatant was collected after 48 hours of normal culture for chemotaxis experiments. $CD8^+$ T cells were resuspended in 200 μL of serum-free culture medium at a density of 1×10^6 cells and added to the upper chamber, while the lower chamber contained 500 μL of tumor supernatant. The cells were incubated for 4 hours. The upper chamber was removed, and 3 random fields of view in the lower chamber were photographed using a phase-contrast microscope to observe the cells that migrated to the lower chamber.

T-cell activation assay

Sorted CD8+ T cells were treated with conditioned media collected from EBV+ ICC cells. After 24 hours of treatment, Brefeldin A was added to block secretion and intracellular expression of IFN-γ, and Granzyme B was assessed by flow cytometry following an additional 24 hours of culture.

cGAMP measurement

cGAMP levels in the cells were measured using the cGAMP kit (Invitrogen, cat# EIAGAMP) according to the manufacturer's instructions.

ELISA

The levels of IL-6, CXCL10, and IFN-γ in cell supernatants and plasma were measured using ELISA kits for IL-6 (Neobioscience, EHC007.96), CXCL10 (Neobioscience, EHC157.96), and IFN-γ (Neobioscience, EHC102g.48) according to the manufacturer's protocols.

In vivo tumorigenesis assay

Female NSG mice (5 week old, Sun Yat-sen University Cancer Center) were randomly divided into 2 groups of 10 mice each. A total of 5×10^6 tumor cells were subcutaneously injected into the right flank of the mice. Tumor formation was monitored, and the mice were euthanized when the tumor volume reached 2 cm^3 or when significant weight loss occurred. The tumors were then collected for subsequent experiments. All relevant procedures were approved by the Institutional Review Board and Ethics Committee of the Sun Yat-sen University Cancer Center (Approval No. L102022023090A).

Proteomics analysis

FFPE tissues were deparaffinized, lysed in buffer (50% ACN, 300 mM Tris-HCl, pH 8.0), sonicated, and heated at 90 °C for 90 minutes for de–cross-linking. Proteins were reduced (5 mM DTT), alkylated (25 mM Cynoacrylic Acid), and digested overnight at 37 °C with trypsin (1:50 ratio). Peptides were acidified (1% TFA), desalted using C18 stage tips, and reconstituted in 0.1% formic acid. LC-MS/MS analysis was performed on a timsTOF Pro mass spectrometer coupled to a nanoElute system, using a 60-minute gradient with a C18 column (75 μm×200 mm, 1.9 μm beads, 120 Å) at 300 nL/min. Data were acquired in dia-PASEF mode and analyzed with DIA-NN 1.8.1 for label-free quantification.

The analysis methods align with those detailed in our previous publication.[8]

Statistical analysis

All experiments were repeated three times. The data shown represent the mean ± SD from at least 3 independent experiments. Statistical analysis was conducted using a two-tailed unpaired Student *t* test in R (v.4.2.2) and GraphPad Prism 8. A p value < 0.05 was considered statistically significant. $^{*}p < 0.05$, $^{**}p < 0.01$, and $^{***}p < 0.001$.

RESULTS

Patients with EBVaICC have a better prognosis with immunotherapy than EBV-negative patients

We reviewed all patients with metastatic cholangiocarcinoma at Sun Yat-sen University Cancer Center from January 2015 to August 2023. Among them, 42 patients had EBER-positive tumor tissue, all of whom were ICC, and 22 of these patients received anti-PD1 treatment. We included 66 patients with EBV-negative ICC (non-EBVaICC) who also received anti-PD1 treatment. The onset of EBVaICC was predominantly female, with a mean age of 51.6 years. HBV infection status and baseline metastatic status were similar to that of non-EBVaICC. The patients included were primarily on first-line immunotherapy (Supplemental Table S2, http://links.lww.com/HC9/B936). The results indicated that among the patients receiving anti-PD1 therapy, EBVaICC had significantly longer median overall survival compared to EBV-negative patients (median overall survival 33.4 vs. 12.4 mo; $p < 0.001$). Similarly, the median progression-free survival (PFS) of EBVaICC was significantly longer than that of EBV-negative patients (median progression-free survival 15.7 vs. 6.5 mo; $p < 0.001$; Figure 1A). EBER in situ hybridization combined with CK7 staining indicated that EBV only infected ICC tumor tissue and did not infect other components in the tumor microenvironment (Figures 1B, C). Here, we exhibited 2 patients with significant reductions in metastatic lesions after anti-PD1 treatment, with one patient achieving a progression-free survival of up to 40.4 months (Figure 1D).

Establishment and validation of EBV-infected ICC cell lines

To establish EBV-infected ICC cell lines, we used EGFP-neo'EBV-infected Akata cells to produce recombinant EBV, co-culturing through the cell-to-cell method. G418 was used to select infected cells, and the GFP positivity of the infected cells was dynamically monitored (Figure 2A). The established EBV-positive ICC cell lines (RBE-EBV and HuH28-EBV) had GFP positivity rates of 69% and 78% (Figures 2B, C). We further assessed the levels of EBV DNA copy numbers in the supernatant and cells of the EBV-positive ICC cell lines, finding that the EBV DNA copy number in RBE-EBV supernatant was 1.5×10^3 copies/μg, and in HuH28-EBV supernatant it was 9.3×10^3 copies/μg. The EBV DNA copy number in RBE-EBV cells was 2.0×10^6 copies/μg, while in HuH28-EBV cells it was 1.6×10^7 copies/μg (Figure 2D). We performed immunohistochemistry staining with the epithelial marker CK7 to exclude residual Akata in EBV-infected cells and further confirmed successful EBV infection through EBER in situ hybridization (Figure 2E).

Latent and lytic reactivation patterns of EBV-positive ICC

Both RBE-EBV and HuH28-EBV cell lines showed expression of latency I genes, represented by EBNA1, EBER1, and EBER2, as well as latency II genes represented by EBNA2, LMP1, and LMP2A. Additionally, latency III genes, represented by EBNA3A, EBNA3B, and EBNA3C, were detected, indicating that the 2 established EBV-positive ICC cell lines exhibit latency III transcriptionally. Moreover, after TPA and NaB induction of lytic reactivation, EBV-related latent genes were upregulated, possibly associated with enhanced EBV replication during lytic reactivation (Figure 3A). With prolonged treatment of TPA and NaB, the immediate-early protein Zta, early protein EA-D, and late lytic protein gp350 were sequentially detected. Although gp350 was not detected in HuH28-EBV in western blot experiments, flow cytometry showed 6.48% positive cells, possibly due to the low expression ratio resulting in insufficient protein for detection by western blot (Figures 3B, C). Similarly, our immunofluorescence further validated the expression of Zta, EA-D, and gp350 post-lytic reactivation (Figure 3D). In summary, RBE-EBV and HuH28-EBV exhibit latency III at the transcriptional level and latency I at the translational level.

Interferon pathway activation and lymphocyte activation in EBV-positive ICC

Enrichment analysis of differentially expressed proteins between tumor and paracancerous tissues from patients with EBVaICC revealed significant enrichment in EBV infection and immune-related pathways (Supplemental Figures S1A, B, http://links.lww.com/HC9/B936). Similarly, differential gene expression analysis

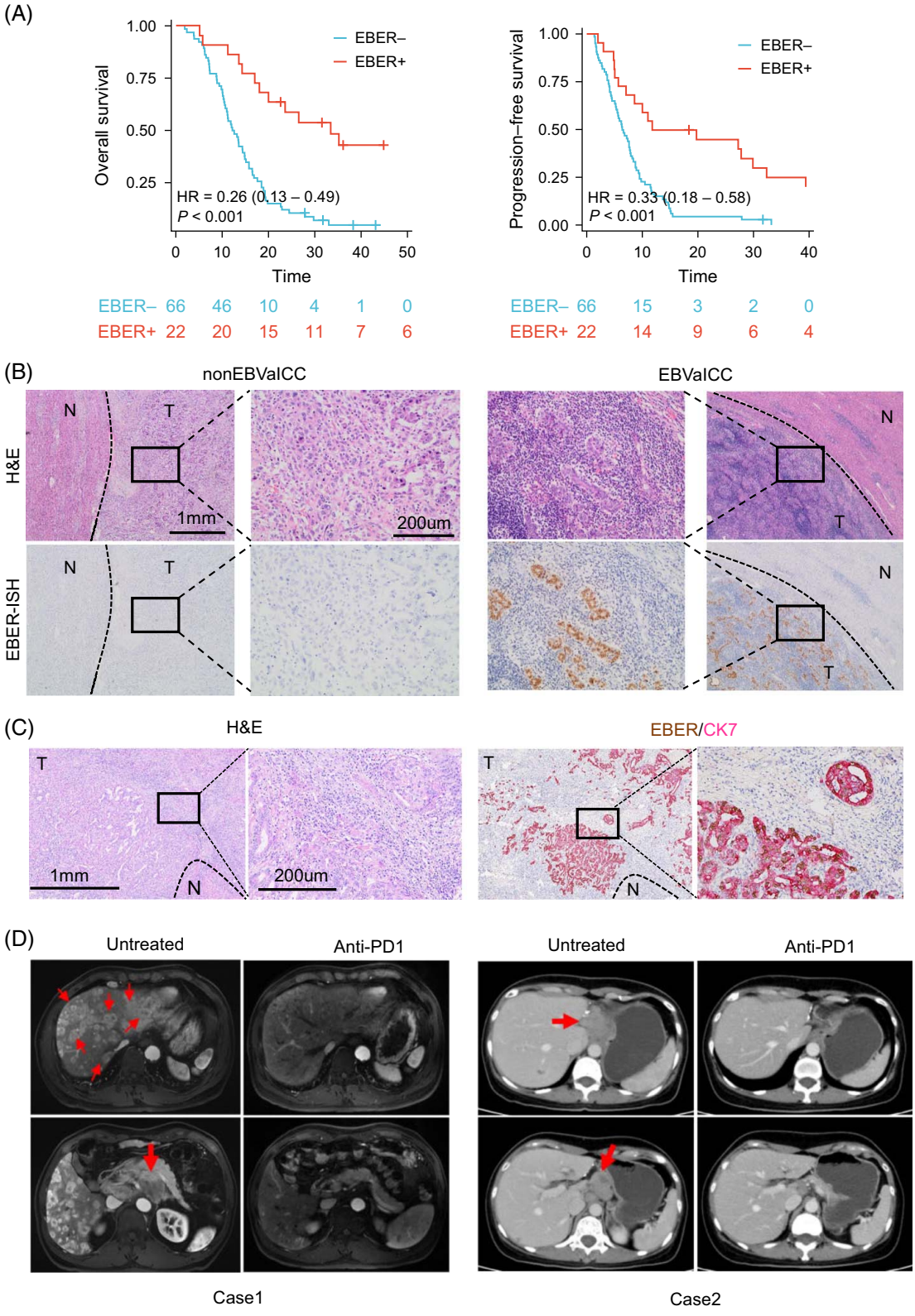

FIGURE 1 Patients with BVaICC demonstrate enhanced immune response compared to patients with non-EBVaICC. (A) Kaplan-Meier survival curves displaying overall survival and progression-free survival of EBER+ (EBV-positive) and EBER− (EBV-negative) patients undergoing anti-PD-1 therapy. (B) Representative images from EBER-ISH staining showing EBV presence in EBVaICC versus non-EBVaICC cases. (C) H&E staining and double staining of EBER (brown) and CK7(red) in EBVaICC. (D) Clinical responses to PD-1 antibody treatment in 2 patients with EBVaICC, showing marked improvement. Abbreviations: EBER-ISH, EBER in situ hybridization; EBVaICC, Epstein-Barr virus–associated intrahepatic cholangiocarcinoma; H&E, Hematoxylin and Eosin; non-EBVaICC, EBV-negative intrahepatic cholangiocarcinoma; PD-1, Programmed cell death protein.

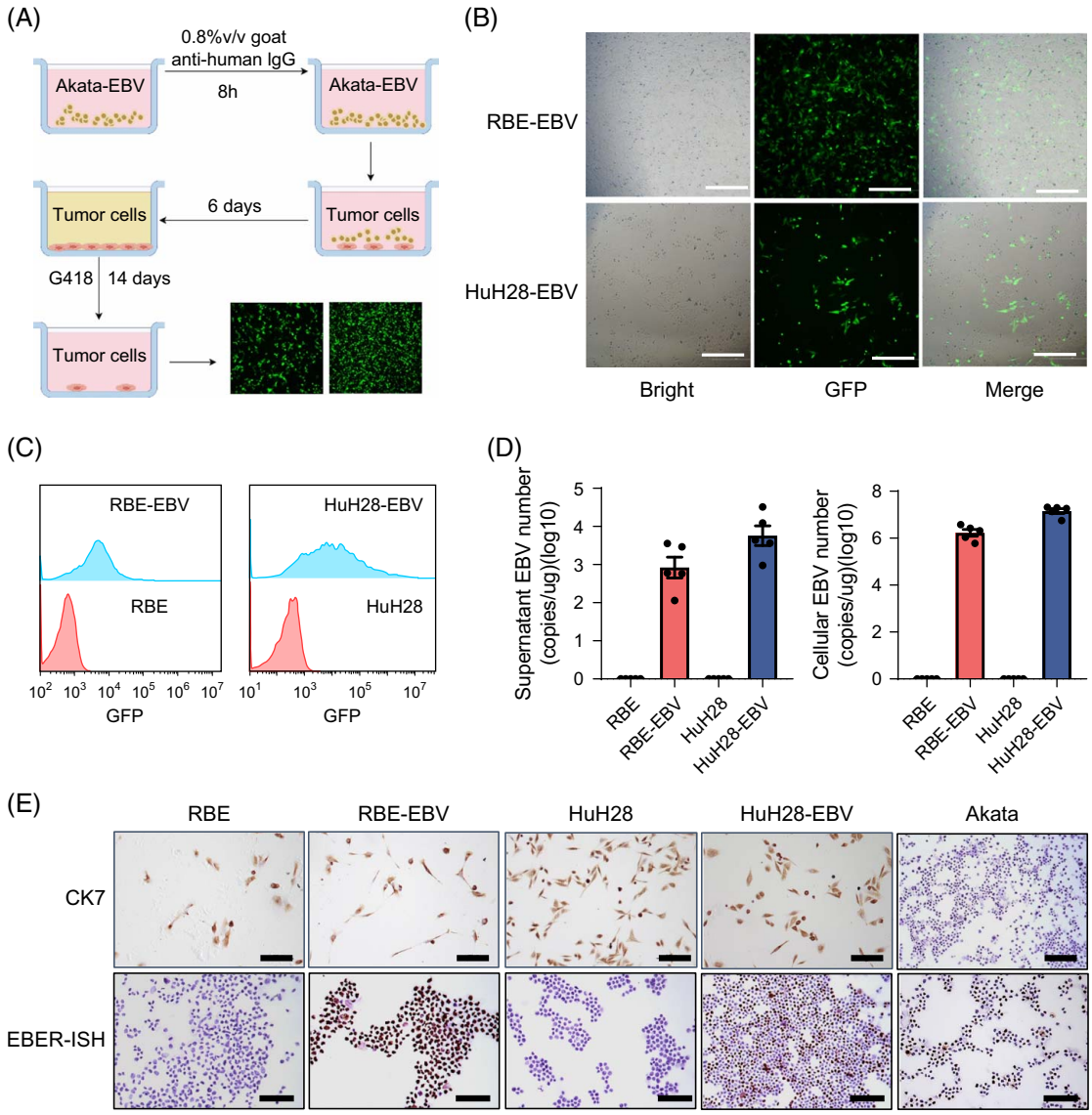

FIGURE 2 Establishment and characterization of EBV-infected intrahepatic cholangiocarcinoma cell lines. (A) Schematic diagram illustrating the establishment process for EBV-positive intrahepatic cholangiocarcinoma cell lines. (B, C) Confirmation of GFP expression in 2 EBV-positive intrahepatic cholangiocarcinoma cell lines (RBE-EBV and HuH28-EBV) via fluorescence microscopy and flow cytometry, indicating successful EBV infection. Scale length: 200 μm. (D) Quantification of EBV DNA copy numbers in cell supernatant and intracellular samples, validating stable viral presence. (E) Immunostaining for CK7 and EBER-ISH in EBV-infected paired cell lines, demonstrating epithelial characteristics and EBV localization. Scale length: 100 μm. Abbreviations: CK7, cytokeratin 7; EBER-ISH, EBER in situ hybridization; EBV, epstein-barr virus; GFP, green fluorescent protein.

through GSEA of RNA-seq data from EBVaICC and non-EBVaICC tissues demonstrated activation of interferon signaling and adaptive immune pathways (Supplemental Figure S1C, D, http://links.lww.com/HC9/B936), indicating a uniquely activated immune microenvironment in patients with EBVaICC.

To further clarify the impact of EBV on the immune microenvironment of ICC and explore the underlying mechanisms, we performed RNA-seq using 2 pairs of EBV-positive ICC cell lines (RBE-EBV and HuH28-EBV) and their parental counterparts. Transcriptome sequencing mapped against the EBV genome confirmed the successful establishment of EBV-positive cell lines and demonstrated the expression of several EBV-related genes (Figure 4A). Differentially expressed genes analysis identified immune-related genes, including CXCL8 and GBP2, as upregulated in both EBV-positive cell lines (Figures 4B, C). The analysis identified 456 overlapping differentially expressed genes by comparing the differentially expressed gene sets of RBE versus RBE-EBV and HuH28 versus HuH28-EBV (Figure 4D). Gene Ontology and Kyoto Encyclopedia of Genes and Genomes enrichment analyses of these intersecting genes revealed predominant enrichment in pathways such as cytokine-cytokine receptor interaction, cytokine-mediated signaling, T-cell

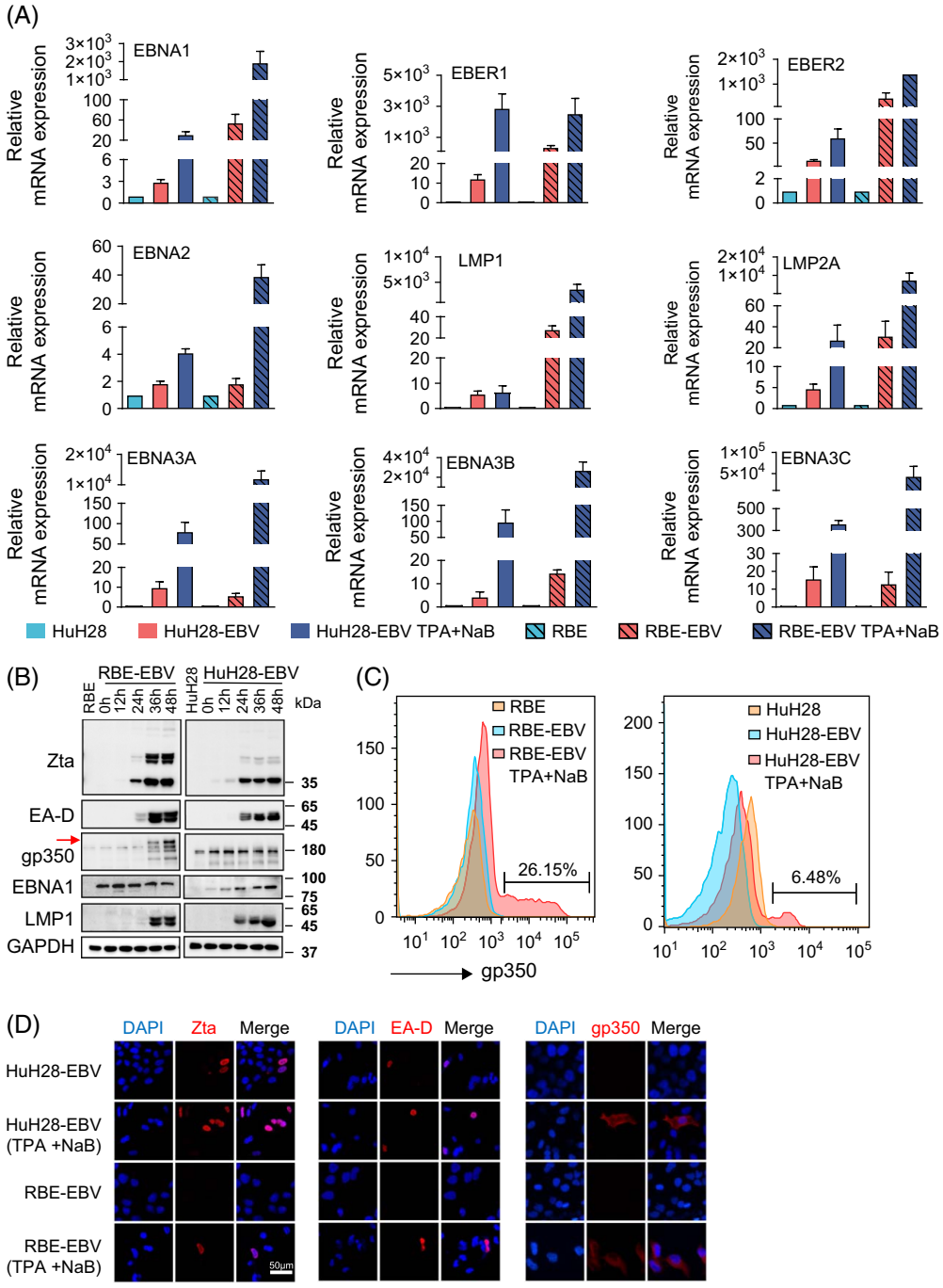

FIGURE 3 Analysis of the EBV life cycle in RBE-EBV and HuH28-EBV cell lines. (A) RT-qPCR analysis of EBV latency gene expression in RBE-EBV and HuH28-EBV cell lines, with and without induction by TPA (20 ng/mL) and NaB (3 mM). (B) Western blot showing the expression of latent and lytic EBV proteins in RBE-EBV and HuH28-EBV cell lines across a time course of TPA (20 ng/mL) and NaB (3 mM) treatment. (C) Flow cytometry analysis of gp350 surface expression in RBE-EBV and HuH28-EBV cell lines before (0 h) and after 48-hour treatment with TPA (20 ng/mL) and/or NaB (3 mM). (D) Immunofluorescence staining for Zta, EA-D, and gp350 in RBE-EBV and HuH28-EBV cell lines at 0 and 48 hours post-treatment with TPA (20 ng/mL) and/or NaB (3 mM). Scale length: 50 μm. Abbreviations: EBV, epstein-barr virus; RT-qPCR, reverse transcription quantitative polymerase chain reaction; TPA, phorbol 12-myristate 13-acetate.

receptor, type I interferon production, and TNF signaling pathways (Figures 4E, F). Similar enrichment patterns were observed in xenograft tumors of HuH28-EBV (Supplemental Figure S2, http://links.lww.com/HC9/B936). Further validation through reverse transcription quantitative polymerase chain reaction confirmed significantly elevated expression of immune-related genes CYFIP2 and GBP2 in RBE-EBV and HuH28-EBV cell lines (Figures 4G, H). These findings reinforce the role of EBV in modulating immune pathways and promoting an immune-activated tumor microenvironment in EBVaICC.

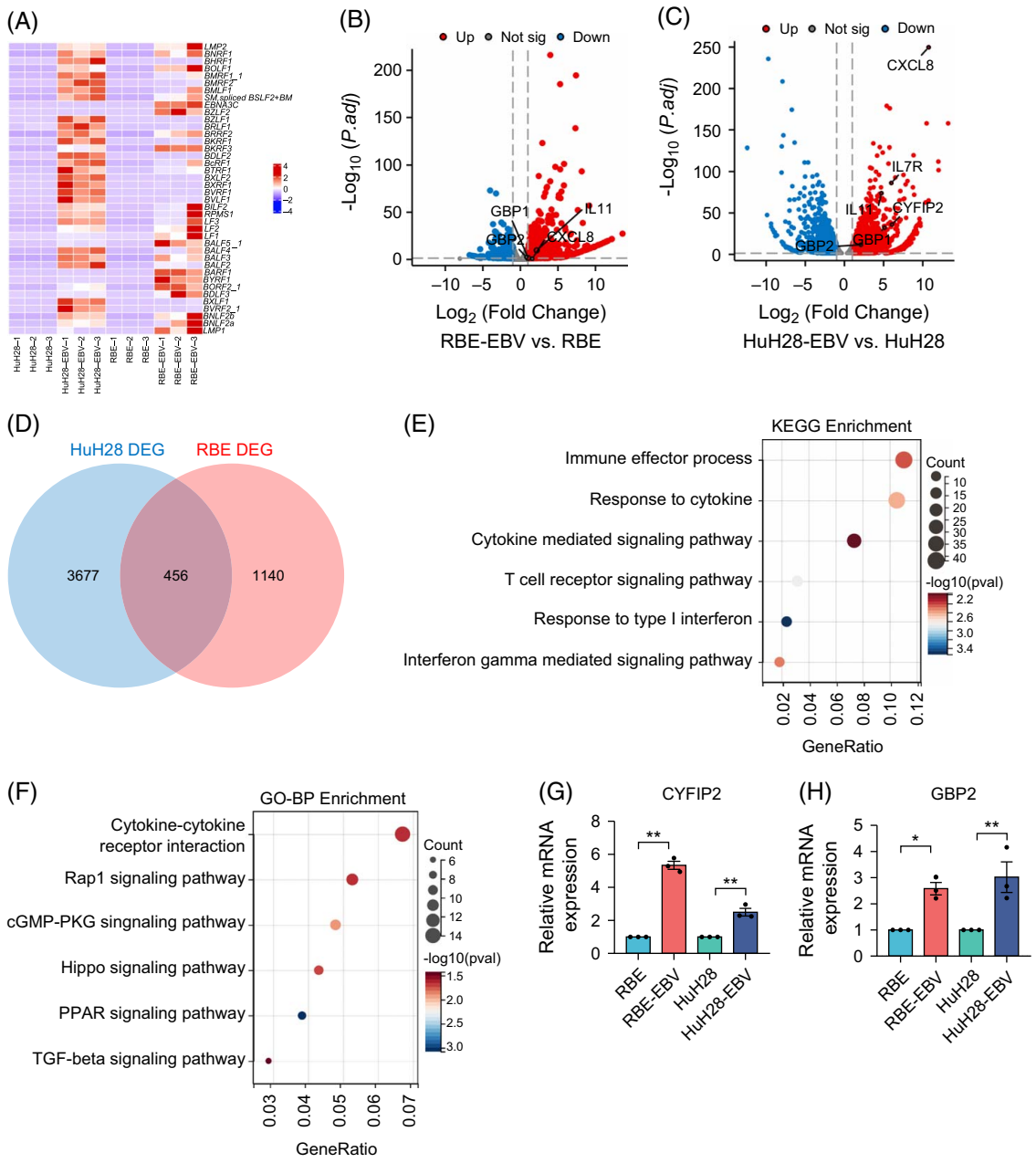

FIGURE 4 Bioinformatics analysis of DEGs in 2 pairs of EBV-positive ICC cell lines. (A) Heatmap of transcriptome sequencing of HuH28, HuH28-EBV, RBE, and RBE-EBV cell lines compared with EBV genome (GCF_002402265.1). (B) Volcano plot of DEGs between RBE-EBV and RBE cell lines. (C) Volcano plot of DEGs between HuH28-EBV and HuH28 cell lines. (D) Venn diagram of intersecting DEGs between 2 pairs of EBV-positive ICC cell lines. (E, F) GO and KEGG enrichment analyses for intersecting DEGs. (G, H) RT-qPCR validation of immune-related genes CYFIP2 and GBP2 in RBE-EBV and HuH28-EBV cell lines. $*p < 0.05$, $**p < 0.01$. Abbreviations: BP, biological process; DEGs, differentially expressed genes; GO, gene ontology; ICC, intrahepatic cholangiocarcinoma; KEGG, kyoto encyclopedia of genes and genomes; RT-qPCR, reverse transcription quantitative polymerase chain reaction.

EBV-positive ICC cells enhance immunotherapy efficacy through cGAS-STING pathway activation and MHC-I upregulation

To further explore the mechanisms behind interferon activation and lymphocyte activation in EBV-positive ICC, we measured the intracellular cGAMP levels and found that RBE-EBV and HuH28-EBV showed increased cGAMP. Subsequently, we assessed the protein levels of p-STING, p-TBK1, and MHC-I in the 2 pairs of EBV cell lines, revealing upregulation in RBE-EBV and HuH28-EBV (Figures 5A, B). Additionally, we analyzed the expression of downstream genes related to the cGAS-STING pathway, finding that IFNA, IFNB1, ISG15, IL6, and CXCL10 were upregulated in RBE-EBV and HuH28-EBV (Figures 5C, D). ELISA confirmed high CXCL10 levels in the supernatants of these EBV-

positive cell lines. We speculate that EBV may promote CXCL10 secretion through activation of cGAS-STING, which promotes T-cell chemotaxis and secretion of IFN-γ, which in turn leads to enhanced T-cell killing ability (Figures 5E–G). ELISA analysis of plasma from 15 pairs of patients with EBVaICC and without EBVaICC showed elevated levels of CXCL10 and IFN-γ in EBVaICC patient plasma, with IL6 also higher, though not statistically significant, supporting our conjecture (Figure 5H). Consistent with our hypothesis, cytotoxicity assays revealed stronger CD8+ T cell activity against EBV-positive cells compared with EBV-negative cells (Figures 6A, B). Furthermore, supernatants from RBE-EBV and HuH28-EBV cells exhibited enhanced chemotactic effects on CD8+ T cells (Figures 6C–E). Conditioned media from EBV+ ICC cells (RBE-EBV and HuH28-EBV) promoted the expression of IFN-γ and Granzyme B in CD8+ T cells (Figures 6F, G).

DISCUSSION

The absence of a representative EBV-positive ICC cell line has limited our understanding of this cancer subtype's molecular and immunologic characteristics. This study highlights that patients with EBVaICC respond favorably to anti-PD-1 therapies, supporting further investigation into the immunological mechanisms driving these outcomes. In this study, we first successfully constructed the EBV-positive ICC line using a cell-to-cell infection method (RBE-EBV and HuH28-EBV). The stable EBV infection and the dynamic responses to viral reactivation within these lines established them as viable models for future EBVaICC research. Preliminary exploration revealed that the immune responsiveness of EBV-positive ICC may arise from cGAS-STING pathway activation, which induces type I interferon signaling, enhances CD8+ T

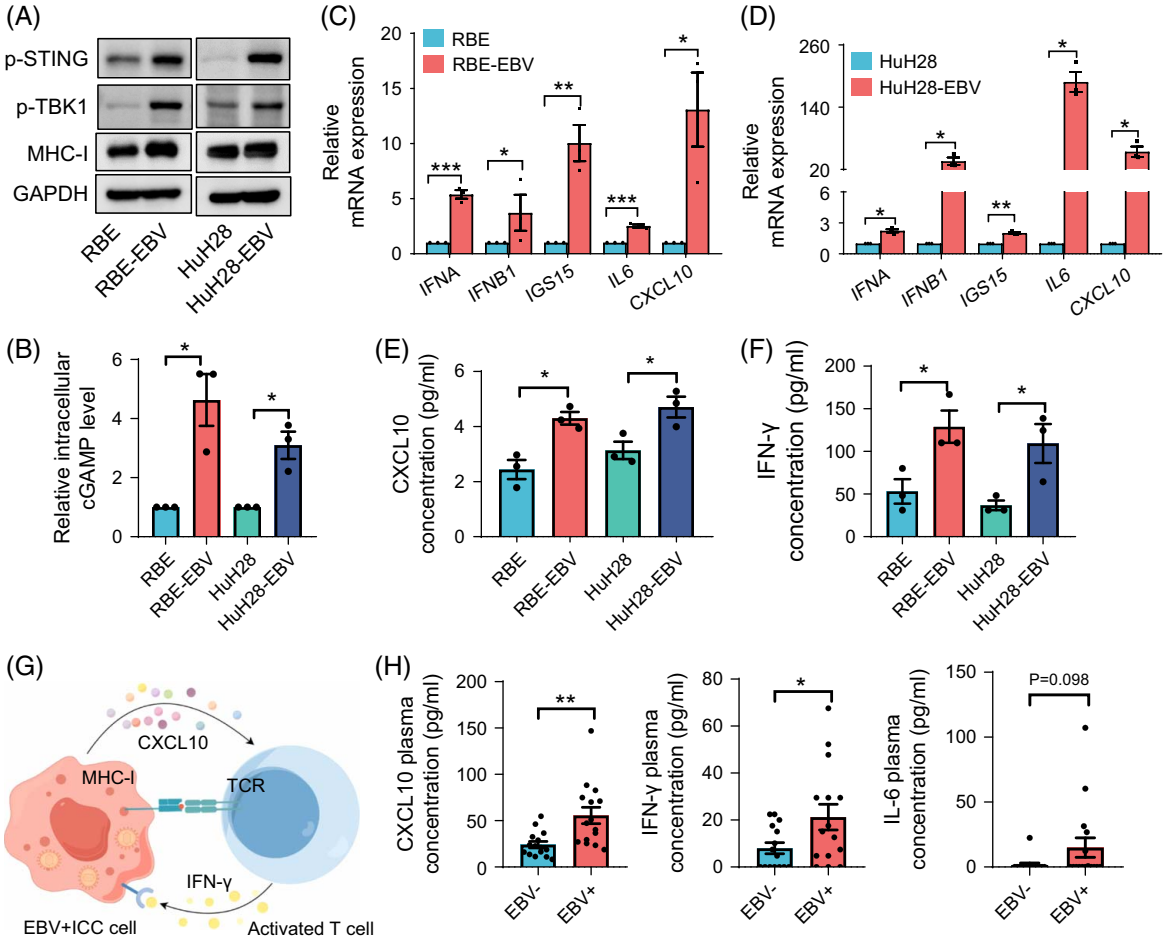

FIGURE 5 Activation of the cGAS-STING pathway by EBV enhances interferon signaling and CXCL10 secretion. (A) Western blot analysis showing increased p-STING, p-TBK1, and MHC-I expression in EBV-positive cell lines compared to EBV-negative counterparts. (B) ELISA quantification of intracellular cGAMP levels in EBV-positive and EBV-negative cell lines. (C, D) RT-qPCR analysis for expression of downstream genes in the cGAS-STING pathway. (E, F) ELISA of CXCL10 and IFN-γ concentrations in the supernatant of cell cultures. (G) Diagram illustrating the paracrine signaling interactions between EBV-positive tumor cells and CD8+ T cells. (H) ELISA measurements of plasma CXCL10, IFN-γ, and IL-6 levels in 15 pairs of EBV-positive and EBV-negative ICC patient samples. *$p < 0.05$, **$p < 0.01$, ***$p < 0.001$. Abbreviations: EBV, epstein-barr virus; ICC, intrahepatic cholangiocarcinoma; MHC-1, major histocompatibility complex class I; RT-qPCR, reverse transcription quantitative polymerase chain reaction; TCR, T cell receptor.

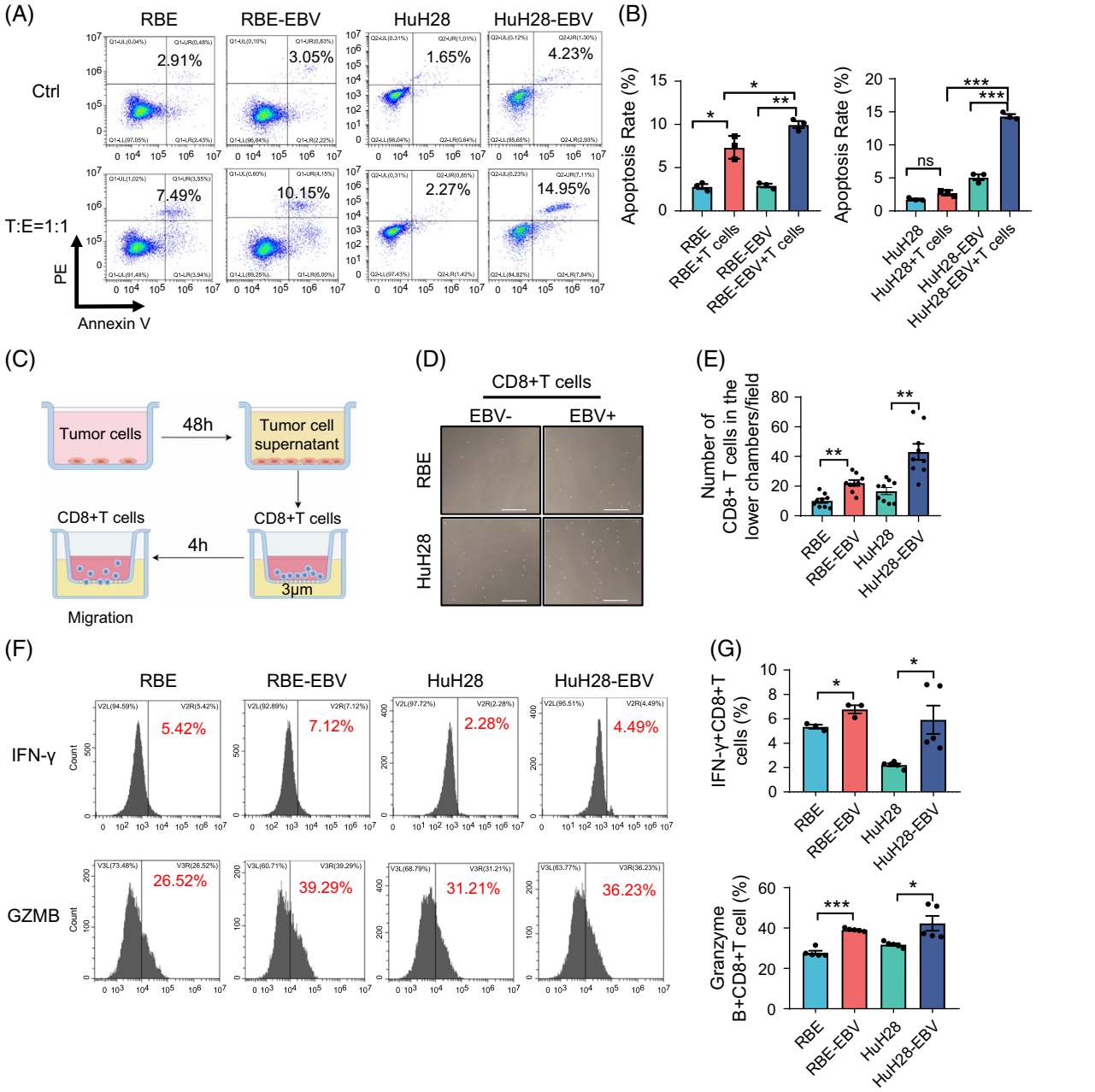

FIGURE 6 EBV infection enhances T-cell–mediated cytotoxicity, T-cell activation, and migration in ICC cells. (A, B) Representative flow cytometry images and quantitative analysis of CD8+ T-cell cytotoxicity 24 hours after co-culture with tumor cells at a 1:1 effector-to-target ratio. (C–E) Assessment of CD8+ T-cell migration induced by supernatants from EBV-positive versus EBV-negative cell lines, measured 4 hours postaddition in transwell assays. Scale length: 50 μm. (F, G) Conditioned media from EBV+ ICC cells (RBE-EBV and HuH28-EBV) activate CD8+ T cells to express IFN-γ and Granzyme B. *$p < 0.05$, **$p < 0.01$, ***$p < 0.001$. Abbreviations: EBV, epstein-barr virus; GZMB, granzyme B.

cell chemotaxis and promotes cytotoxic effects on tumor cells.

Maintaining the EBV genome within a cell line is fundamental to establishing EBV-positive cell models. Both the RBE -EBV and HuH28-EBV cell lines sustained the EBV genome and expressed EBERs along with both latent and lytic genes, although expression levels varied between the lines. EBV exhibits dynamic transitions between latent and lytic cycles during host cell infection. In the latent phase, EBV DNA circularizes in the host nucleus and is silenced through chromatin modifications, such as H3K27me3, and progressive CpG methylation of lytic genes.[21,22] This ensures the long-term persistence of the virus. During latency, only a limited number of genes, such as EBNA1, are expressed. These genes maintain the stability of the viral genome and facilitate its equal segregation during cell division by tethering the viral DNA to host chromatin via the oriP region.[23,24] Under specific stimuli, such as antigenic stimulation,

EBV can reactivate from latency and enter the lytic phase. The lytic cycle is initiated by the expression of key immediate-early genes, including BZLF1 and BRLF1, which disrupt the silencing of lytic genes and trigger a cascade of downstream lytic gene expression. The viral DNA undergoes replication at the oriLyt region, and the assembled viral particles are released via cell lysis or exocytosis, enabling infection of new host cells.[25,26] This ability to alternate between latency and lytic reactivation ensures the virus's long-term persistence and transmission while evading the host's immune response. This unique feature profoundly influences the tumor microenvironment and immune landscape in EBV-associated cancers. In EBV-associated cancers, these dynamics significantly impact the tumor microenvironment and immune landscape. Previous clinical research indicated that EBVaICC displays a latency I, limited to EBNA1 expression. However, in addition to EBNA1, our newly established HuH28-EBV and RBE-EBV cell lines exhibited RNA transcripts for other latency genes (EBNA2, EBNA3A, EBNA3B, EBNA3C, LMP1, and LMP2A), suggesting that EBV latency patterns in ICC may extend beyond the conventional latency I. Further, RNA-seq of the paired RBE cell lines detected sporadic expression of lytic genes (BALF5, BMRF1, BRLF1, BMLF1, BALF4), indicating that EBV-positive ICC cells can undergo lytic activation under appropriate conditions, consistent with findings in nasopharyngeal and gastric carcinomas.[27–29] Treatment with TPA and NaB triggered reactivation in HuH28-EBV and RBE-EBV, confirmed by Zta and EA-D expression, indicating dynamic viral life cycle engagement.

The interferon pathway is crucial for antiviral and antitumor immunity.[30–33] Our findings indicated that EBV infection activated the IFN pathway within ICC cell lines, inducing IFN-α and IFN-β expression, enhancing antiviral states, and stimulating adaptive immunity. Type I IFNs initiate expression of antiviral and proinflammatory genes through the IFN-α/β receptor and the Janus Kinase-Signal Transducer and Activator of Transcription pathway.[34] RIG-I, which recognized EBV-derived EBER, triggered signaling pathways to induce IFN production within infected cells.[35] EBV also stimulated plasmacytoid dendritic cells to secrete IFN-α, activating both natural killer cells and T cells.[36] These findings indicated that EBV infection could play a critical role in promoting antitumor immunity within the tumor microenvironment.

To determine the mechanism driving interferon pathway activation, we observed that cGAS-STING signaling was upregulated in EBV-positive ICC cell lines, evidenced by increased cGAMP levels. The cGAS-STING pathway is a key cytosolic DNA sensor that activates immune responses, largely through the induction of type I IFNs and proinflammatory cytokines.[17] The STING protein is central to antiviral innate immune signaling and is regarded as a pivotal regulator of antiviral and antitumor immunity.[37] Through cGAS-STING activation, EBV may enhance tumor immunity by promoting CD8+ T-cell migration and activity, thereby curtailing tumor cell proliferation.[38] This mechanism provides insight into the immunotherapeutic sensitivity observed in EBV-positive ICC. Additionally, EBV's deubiquitinase BPLF1 may dampen cGAS-STING-mediated IFN production,[19] suggesting that EBV may employ complex host modulation strategies to sustain infection. The dual impact of EBV on this pathway warrants further investigation.

Next, our data showed that interferon pathway-associated genes were activated in RBE-EBV and HuH28-EBV and that CXCL10 levels were elevated in the supernatants of EBV-positive cell lines and the plasma of patients with EBVaICC. CXCL10, a key chemokine that recruits CXCR3+ CD8+ T cells, contributes to creating "hot" tumors responsive to checkpoint inhibitors.[39] Produced by antigen-presenting cells, macrophages, and tumor cells, CXCL10 facilitates T-cell infiltration, essential for effective immunotherapy. This process creates a feedback loop, where T cells secrete IFN-γ, further amplifying CXCL10 production and immune cell recruitment, supporting immune response and therapy efficacy.[39,40] Consistently, higher IFN-γ levels were observed in EBVaICC patient plasma in our study, suggesting EBV might remodel the immune microenvironment by enhancing CXCL10 production.

EBV-specific CD8+ T cells have shown antitumor effects in low-immunogenic hematologic malignancies, with promising applications in EBV-associated solid tumors.[41,42] Our previous work showed elevated CD8+ T-cell infiltration and PD-L1 expression in the tumor microenvironment of EBVaICC.[8] Here, we demonstrated that supernatants from EBV-positive ICC cells promote CD8+ T-cell migration, likely due to elevated IFN production. Type I IFN signaling indirectly enhances EBV-specific CD8+ T-cell cytokine production and can suppress viral replication early in infection to partially preserve IFN signaling function.[43] CD8+ T-cell responses are critical in controlling EBV-associated replication and reactivation, and these cells may suppress EBV-related malignancies.[44,45]

The EBV-positive ICC cell lines established in this study present promising models for preclinical research. While our findings illuminate key immunological aspects of EBV-positive ICC, cell line models have inherent limitations in replicating the complexity of in vivo tumor microenvironments. Future studies should incorporate patient-derived organoids or humanized animal models to further delineate the immune regulatory mechanisms in EBV-positive ICC. Moreover, further research is necessary to clarify the roles of IFN and cGAS-STING pathways in EBV infection, ultimately supporting the development of individualized therapies for EBVaICC.

CONCLUSIONS

The established EBV-positive ICC cell lines revealed enhanced immunogenicity driven by cGAS-STING pathway activation, providing valuable models for future research and insights into the mechanisms of improved immunotherapy sensitivity in EBVaICC.

DATA AVAILABILITY STATEMENT

All data used in this work was available from the corresponding author upon reasonable request. The raw sequence data reported in this paper have been deposited in the Genome Sequence Archive of the BIG Data Center at the Beijing Institute of Genomics, Chinese Academy of Sciences, under project number PRJCA036980 (http://bigd.big.ac.cn/gsa-human). The code is available from the corresponding author upon reasonable request.

AUTHOR CONTRIBUTIONS

Lingli Huang: methodology, formal analysis, writing—original draft, visualization, and writing—review and editing. Silan Huang and Kejia Yang: investigation, software, supervision, and data curation. Qian Zhong and Yuchen Cai: methodology and supervision. Guifang Guo: conceptualization, supervision, and funding acquisition.

FUNDING INFORMATION

This study was supported by the Natural Science Foundation of Guangdong Province (2021A1515012368; 2023A1515010783).

ACKNOWLEDGMENTS

The authors thank Prof Shengping Li at Sun Yat-sen University Cancer Center for the generous provision of the RBE and HuH28 cell lines, Prof Lin Feng at Sun Yat-sen University Cancer Center for invaluable scientific guidance, to Specimen Resource Library at Sun Yat-sen University Cancer Center for providing Tissue and plasma samples, and Prof Musheng Zeng at Sun Yat-sen University Cancer Center for supplying the Raji and Akata cell lines. Pattern diagram drawn by figdraw.

CONFLICTS OF INTEREST

The authors have no conflicts to report.

REFERENCES

1. Kam AE, Masood A, Shroff RT. Current and emerging therapies for advanced biliary tract cancers. Lancet Gastroenterol Hepatol. 2021;6:956–69.
2. Rimini M, Fornaro L, Rizzato MD, Antonuzzo L, Rossari F, Satake T, et al. Durvalumab plus gemcitabine and cisplatin in advanced biliary tract cancer: A large real-life worldwide population. Eur J Cancer. 2024;208:114199.
3. Burris HA III, Okusaka T, Vogel A, Lee MA, Takahashi H, Breder V, et al. Durvalumab plus gemcitabine and cisplatin in advanced biliary tract cancer (TOPAZ-1): Patient-reported outcomes from a randomised, double-blind, placebo-controlled, phase 3 trial. Lancet Oncol. 2024;25:626–35.
4. Khan SA, Tavolari S, Brandi G. Cholangiocarcinoma: Epidemiology and risk factors. Liver Int. 2019;39(suppl 1):19–31.
5. Yoon JG, Kim MH, Jang M, Kim H, Hwang HK, Kang CM, et al. Molecular Characterization of biliary tract cancer predicts chemotherapy and programmed death 1/programmed death-ligand 1 blockade responses. Hepatology. 2021;74: 1914–31.
6. Scott AJ, Sharman R, Shroff RT. Precision medicine in biliary tract cancer. J Clin Oncol. 2022;40:2716–34.
7. Huang YH, Zhang CZ, Huang QS, Yeong J, Wang F, Yang X, et al. Clinicopathologic features, tumor immune microenvironment and genomic landscape of Epstein-Barr virus-associated intrahepatic cholangiocarcinoma. J Hepatol. 2021; 74:838–49.
8. He WZ, Huang YH, Hu WM, Wang F, Xu YX, Yi JH, et al. Response to programmed cell death protein 1 antibody in patients with Epstein-Barr virus-associated intrahepatic cholangiocarcinoma. Eur J Cancer. 2023;194:113337.
9. Farrell PJ. Epstein-Barr virus and cancer. Annu Rev Pathol. 2019;14:29–53.
10. Epstein MA, Achong BG, Barr YM. Virus particles in cultured lymphoblasts from Burkitt's lymphoma. Lancet. 1964;1:702–3.
11. Granucci F, Zanoni I, Pavelka N, van Dommelen SLH, Andoniou CE, Belardelli F, et al. A contribution of mouse dendritic cell-derived IL-2 for NK cell activation. J Exp Med. 2004;200:287–95.
12. Iwakiri D, Zhou L, Samanta M, Matsumoto M, Ebihara T, Seya T, et al. Epstein-Barr virus (EBV)-encoded small RNA is released from EBV-infected cells and activates signaling from Toll-like receptor 3. J Exp Med. 2009;206:2091–9.
13. Ariza ME, Glaser R, Kaumaya PTP, Jones C, Williams MV. The EBV-encoded dUTPase activates NF-kappa B through the TLR2 and MyD88-dependent signaling pathway. J Immunol. 2009;182: 851–9.
14. Glaser R, Litsky ML, Padgett DA, Baiocchi RA, Yang EV, Chen M, et al. EBV-encoded dUTPase induces immune dysregulation: implications for the pathophysiology of EBV-associated disease. Virology. 2006;346:205–18.
15. Shen Y, Zhang S, Sun R, Wu T, Qian J. Understanding the interplay between host immunity and Epstein-Barr virus in NPC patients. Emerg Microbes Infect. 2015;4:e20.
16. Lu C, Guan J, Lu S, Jin Q, Rousseau B, Lu T, et al. DNA sensing in mismatch repair-deficient tumor cells is essential for anti-tumor immunity. Cancer Cell. 2021;39:96–108.e6.
17. Stempel M, Chan B, Brinkmann MM. Coevolution pays off: Herpesviruses have the license to escape the DNA sensing pathway. Med Microbiol Immunol. 2019;208:495–512.
18. Duan Y, Li S, Huang B, Dou Y, Kong P, Kang W, et al. CD47-targeted immunotherapy unleashes antitumour immunity in Epstein-Barr virus-associated gastric cancer. Clin Immunol. 2023;247:109238.
19. Lui WY, Bharti A, Wong NHM, Jangra S, Botelho MG, Yuen KS, et al. Suppression of cGAS- and RIG-I-mediated innate immune signaling by Epstein-Barr virus deubiquitinase BPLF1. PLoS Pathog. 2023;19:e1011186.
20. Imai S, Nishikawa J, Takada K. Cell-to-cell contact as an efficient mode of Epstein-Barr virus infection of diverse human epithelial cells. J Virol. 1998;72:4371–8.
21. Woellmer A, Arteaga-Salas JM, Hammerschmidt W. BZLF1 governs CpG-methylated chromatin of Epstein-Barr Virus reversing epigenetic repression. PLoS Pathog. 2012;8:e1002902.
22. Buschle A, Hammerschmidt W. Epigenetic lifestyle of Epstein-Barr virus. Semin Immunopathol. 2020;42:131–42.
23. Gahn TA, Sugden B. An EBNA-1-dependent enhancer acts from a distance of 10 kilobase pairs to increase expression of the Epstein-Barr virus LMP gene. J Virol. 1995;69:2633–6.

24. De Leo A, Calderon A, Lieberman PM. Control of viral latency by episome maintenance proteins. Trends Microbiol. 2020;28:150–62.
25. Flemington E, Speck SH. Autoregulation of Epstein-Barr virus putative lytic switch gene BZLF1. J Virol. 1990;64:1227–32.
26. Bergbauer M, Kalla M, Schmeinck A, Göbel C, Rothbauer U, Eck S, et al. CpG-methylation regulates a class of Epstein-Barr virus promoters. PLoS Pathog. 2010;6:e1001114.
27. Tsai MH, Raykova A, Klinke O, Bernhardt K, Gärtner K, Leung CS, et al. Spontaneous lytic replication and epitheliotropism define an Epstein-Barr virus strain found in carcinomas. Cell Rep. 2013;5:458–70.
28. Jung YJ, Choi H, Kim H, Lee SK. MicroRNA miR-BART20-5p stabilizes Epstein-Barr virus latency by directly targeting BZLF1 and BRLF1. J Virol. 2014;88:9027–37.
29. Strong MJ, Xu G, Coco J, Baribault C, Vinay DS, Lacey MR, et al. Differences in gastric carcinoma microenvironment stratify according to EBV infection intensity: Implications for possible immune adjuvant therapy. PLoS Pathog. 2013;9:e1003341.
30. Ivashkiv LB, Donlin LT. Regulation of type I interferon responses. Nat Rev Immunol. 2014;14:36–49.
31. McNab F, Mayer-Barber K, Sher A, Wack A, O'Garra A. Type I interferons in infectious disease. Nat Rev Immunol. 2015;15:87–103.
32. Welsh RM, Bahl K, Marshall HD, Urban SL. Type 1 interferons and antiviral CD8 T-cell responses. PLoS Pathog. 2012;8:e1002352.
33. Guo G, Wang Y, Zhou Y, Quan Q, Zhang Y, Wang H, et al. Immune cell concentrations among the primary tumor microenvironment in colorectal cancer patients predicted by clinicopathologic characteristics and blood indexes. J Immunother Cancer. 2019;7:179.
34. Majoros A, Platanitis E, Kernbauer-Hölzl E, Rosebrock F, Müller M, Decker T. Canonical and non-canonical aspects of JAK-STAT signaling: Lessons from interferons for Cytokine Responses. Front Immunol. 2017;8:29.
35. Samanta M, Iwakiri D, Kanda T, Imaizumi T, Takada K. EB virus-encoded RNAs are recognized by RIG-I and activate signaling to induce type I IFN. Embo j. 2006;25:4207–14.
36. Lim WH, Kireta S, Russ GR, Coates PTH. Human plasmacytoid dendritic cells regulate immune responses to Epstein-Barr virus (EBV) infection and delay EBV-related mortality in humanized NOD-SCID mice. Blood. 2007;109:1043–50.
37. Zhang C, Ye S, Ni J, Cai T, Liu Y, Huang D, et al. STING signaling remodels the tumor microenvironment by antagonizing myeloid-derived suppressor cell expansion. Cell Death Differ. 2019;26:2314–28.
38. Fitzgerald KA, McWhirter SM, Faia KL, Rowe DC, Latz E, Golenbock DT, et al. IKKepsilon and TBK1 are essential components of the IRF3 signaling pathway. Nat Immunol. 2003;4:491–6.
39. Reschke R, Gajewski TF. CXCL9 and CXCL10 bring the heat to tumors. Sci Immunol. 2022;7:eabq6509.
40. Ben-Baruch A. The multifaceted roles of chemokines in malignancy. Cancer Metastasis Rev. 2006;25:357–71.
41. Comoli P, Pedrazzoli P, Maccario R, Basso S, Carminati O, Labirio M, et al. Cell therapy of stage IV nasopharyngeal carcinoma with autologous Epstein-Barr virus-targeted cytotoxic T lymphocytes. J Clin Oncol. 2005;23:8942–9.
42. Tzannou I, Papadopoulou A, Naik S, Leung K, Martinez CA, Ramos CA, et al. Off-the-shelf virus-specific T cells to treat BK virus, human herpesvirus 6, cytomegalovirus, Epstein-Barr virus, and adenovirus infections after allogeneic hematopoietic stem-cell transplantation. J Clin Oncol. 2017;35:3547–57.
43. Jennings RN, Grayson JM, Barton ES. Type I interferon signaling enhances CD8+ T cell effector function and differentiation during murine gammaherpesvirus 68 infection. J Virol. 2014;88:14040–9.
44. Ramos da Silva S, Elgui de Oliveira D. HIV, EBV and KSHV: Viral cooperation in the pathogenesis of human malignancies. Cancer Lett. 2011;305:175–85.
45. Icheva V, Kayser S, Wolff D, Tuve S, Kyzirakos C, Bethge W, et al. Adoptive transfer of epstein-barr virus (EBV) nuclear antigen 1-specific t cells as treatment for EBV reactivation and lymphoproliferative disorders after allogeneic stem-cell transplantation. J Clin Oncol. 2013;31:39–48.

How to cite this article: Huang L, Zhong Q, Huang S, Yang K, Cai Y, Guo G. EBV enhances immunotherapy sensitivity in intrahepatic cholangiocarcinoma through cGAS-STING pathway activation. Hepatol Commun. 2025;9:e0674. https://doi.org/10.1097/HC9.0000000000000674